Computational Materials Science 47 (2009) 71–78

Contents lists available at ScienceDirect

Computational Materials Science

journal homepage: www.elsevier.com/locate/commatsci

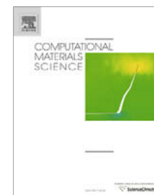

Effective diffusivity of lead free solder alloys

Shidong Li *, Cemal Basaran

Electronic Packaging Laboratory, State University of New York at Buffalo, NY 14260, United States

ARTICLE INFO

Article history:
Received 11 March 2009
Received in revised form 10 June 2009
Accepted 17 June 2009
Available online 21 July 2009

PACS:
31.15.xv

Keywords:
Monte Carlo
Effective diffusivity
Lead free solder alloys
Multi-scale modeling

ABSTRACT

A Monte Carlo simulation based algorithm is developed to compute the effective diffusivity of lead free solder alloys. Simulations are performed to determine the vacancy diffusivity for 95.5Sn–4.0Ag–0.5Cu (SAC405) solder alloy for different paths. Temperature and micro-structural influence on diffusivity are studied. A map of diffusivity versus temperature and average grain size is developed. Significant differences between diffusivity values reported in the literature for the same solder alloy is also discussed.

© 2009 Elsevier B.V. All rights reserved.

1. Introduction

Numerical simulation is very powerful and widely used in material modeling. However, the reliability of a numerical simulation depends greatly on the understanding of the physical/chemical mechanisms, and the material property values used as input. Precise material properties are as important as accurate governing equations in many cases. Garbage-In-Garbage-Out is a well known term among computational mechanists In the literature, for constitutive modeling of lead free solder alloys, some of the material properties have been obtained by experiments; however, some of the very important ones are either not available or reported values vary significantly from one reference to other. Diffusion coefficient value is one of the most critical material properties that affect electromigration (EM), thermomigration (TM) and creep analysis of solder alloys because of their very low melting temperature (about 220 °C). It is well known that metals exhibit significant diffusivity at temperatures above $0.4T_m$ [1] One of the reasons for variation in the reported values is the extreme difficulty in measuring diffusivity properties along different diffusion paths independently.

Experiments usually provide an average value of diffusivity but do not yield any information about the contribution of lattice, lattice defect, grain boundary and surface diffusivities. Gleixner et al [2,3] reported that lattice strain due to electromigration is too small and lattice diffusion is too slow to nucleate a void in passivated interconnect lines according to established electromigration theories. However, they observed that voids nucleate much faster than theoretical prediction. Authors attributed this discrepancy between theory and experimental observations to interface flaws and interface contaminations. Basaran et al [4,5] have shown that void nucleation due to thermomigration in solder alloys is governed by the fastest diffusing constituents transport along the fastest path rather than the average diffusivity of the matrix (host component) and solute. However, in a macro-scale finite element analysis it is not feasible to discretize a solder joint at the atomic level. Molecular Dynamic Simulations (MDS) can provide a glimpse of these different diffusion paths used by different constituents. However, MDS is limited to very short time frame (femtosecond range). As a result "a rare event" like diffusion cannot be observed as a function of time in MDS. Another drawback of MDS is the limitation of number of atoms and grain boundaries that can be included in a single analysis. Therefore, MDS are usually either for lattice or for grain boundary, but not across both regions which would represent inhomogenity of the matrix at the atomic scale.

In a macro-scale finite element analysis of a nanoelectronics packaging solder joints an average diffusivity value must be used because of computational cost of modeling at the atomic resolution, Fig. 1a. However, if we could discretize at a higher resolution, different constituents and their boundaries and initial defects would yield different diffusivities (Fig. 1b). Going one step further in higher resolution would allow us to account for all diffusion paths independently. Fig. 1c shows a grain boundary and lattice interface. At this scale each region can be characterized by a separated set of properties.

* Corresponding author.
E-mail address: shidongli@gmail.com (S. Li).

0927-0256/$ - see front matter © 2009 Elsevier B.V. All rights reserved.
doi:10.1016/j.commatsci.2009.06.015

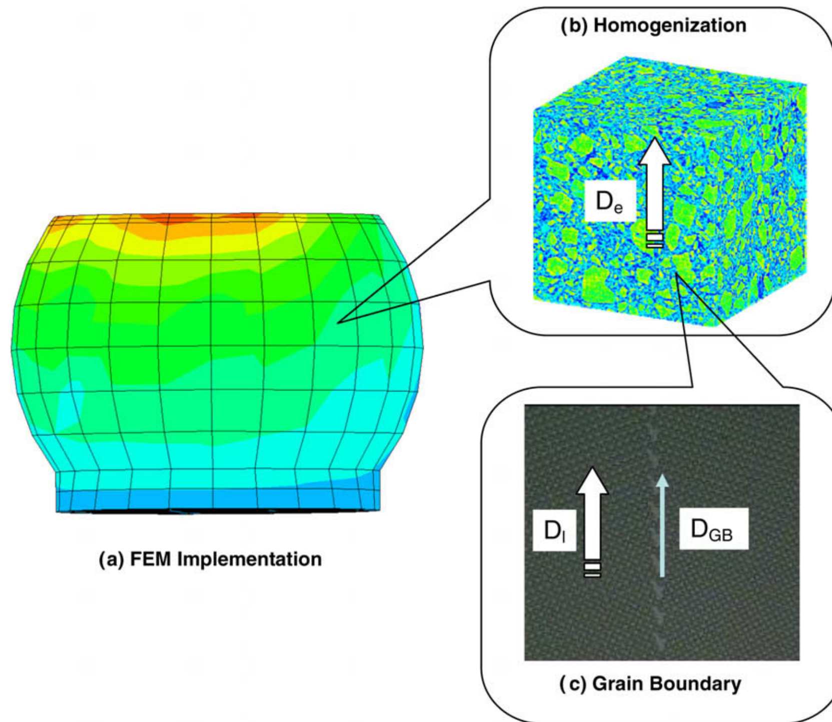

Fig. 1. Dimension gaps of multi-scale material modeling.

Typical size of nanoelectronics packaging solder joint is in micron scale, while the typical grain boundary width is about 0.5 nm. Although the 0.5 nm width grain boundary is negligible in dimension, its contribution to diffusion is significant [6]. The existence of grain boundaries actually plays a major role in diffusion process in polycrystalline material such as solder alloys. Therefore, a single solder joint, needs to be meshed up to 10^6 elements in each direction to be able to simulate the change of the continuity, which is impossible. Therefore, a homogenized effective diffusivity value, which accounts for all diffusion paths, is needed for a multi-scale macro scale analysis.

By measuring the intermetallic (IMC) growth, Arrhenius relationship was used to determine the activation energies for SAC405 lead free solder alloy, as shown in Table 1. However, these varying values actually represent the properties of the IMC layer at the interface, which is significantly different than solder alloy itself. No effective diffusivity value for solder alloy SAC405 has been reported in the literature. In most studies diffusivity of SAC405 is assumed to be the same as that of pure tin because tin makes up 95.5% by weight of the entire composition, [7,8]. This simplification is not accurate and is not supported by any experimental evidence. It has been shown by Abdulhamid et al. [9] and Li et al. [10] that although 95.5% of the composition for SAC405 is tin, copper(0.5%) and silver(4.0%), effective mass transport and degradation is still dominated by the fastest diffusing atoms during electromigration and thermomigration processes. Therefore, it is not reasonable to use the value of pure tin as an approximation for SAC405. In this paper, a method is proposed to compute the diffusivity of SAC405 (Sn95.5/Ag4.0/Cu/0.5 by weight) using Monte Carlo simulations and experimental data. The proposed methodology allows the user to predict diffusivity based on different variations of microstructure, initial defects and variations in grain boundaries.

Table 1
Activation energy for SnAgCu solder alloy as reported in the literature.

Q (Kcal mol^{-1})	Ref.
16.5	Allen [11]
20.6	Dariavach [12]
19.3	Gee [13]
17.4	Xu [14]

Monte Carlo simulation [15] is a procedure in which random numbers are generated according to probabilities assumed to be associated with a source of uncertainty [16]. It is a widely used class of computational algorithm for simulating the behavior of various physical and mathematical systems. Monte Carlo methods are distinguished from other simulation methods (such as molecular dynamics simulations) by being stochastic as opposed to deterministic algorithms.

The term Monte Carlo method describes a large class of approaches with the following common characters;

1. develop a probability model or a random process associated to the target problem;
2. define a domain of possible inputs and generate inputs randomly from the domain;
3. perform a deterministic computation on the given inputs;
4. aggregate the results of the individual computations into the final results;
5. use the statistical characteristics as the approximation solution and error estimate for the real problem.

Based on these principles a simulation methodology has been developed to estimate effective diffusivity of SAC405 solder for different microstructures.

2. Atomic view of diffusion

A profound observation was made by Robert Brown in 1827 that small particles suspended in an isothermal fluid move randomly. Brownian motion had been an experimental confusion and philosophical debate for more than 75 years until Albert Einstein came up with his theory in 1905 [17]. In this paper, Einstein used his hypothesis to show the consistency of random motions of macroscopic particles with the presence of molecules

in the suspending fluid. He reasoned that molecules comprising any phase of matter are always subject to thermodynamic fluctuations of a purely statistical nature. These fluctuations provide the motivating source of stochastic motions occurring in matter all the way down to the atomic scale. The molecular view of diffusion finally lead to an important statistical mechanical concept called random walk. A random walk is a mathematical formalization of a trajectory that consists of taking successive steps in random directions. Most generally, random walks are any stochastic process where the position of a particle at a certain time depends only on its position at some previous time and some random variable which determines its subsequent step length and direction.

Using the concept of random walk, the cumulative distribution surrounding an instantaneous point source in three dimensions is deduced by Glicksman [18], which finally yields a relationship between the root-mean-square displacement of the diffusion cloud and the diffusion parameter as shown

$$\langle R^2\rangle^{1/2} = \sqrt{6Dt} \tag{1}$$

In solder alloy SAC405, there are three constituents with different diffusion coefficients. Considering an instantaneous point source located at the origin, $r = 0$, at the initial time $t = 0$. After a period of time, the different diffusants will spread at a different range according to their inherent diffusivity, as is illustrated in Fig. 2.

By assuming that in the mixture, the occurrence probability for each diffusion couple is proportional to their mole percentage, or the fraction of number of atoms. After simple algorithm operation, we have

$$\langle R^2\rangle = \sum_{i=1}^{m}\sum_{j=1}^{m} n_i n_j \langle R^2\rangle_{ij} \tag{2}$$

where n_i, n_j are mole percentage of the ith and jth component individually; $\langle R^2\rangle_{ij}$ stands for the mean-square-radial displacement for the ith and jth components.

Eq. (2) inevitably yields that

$$D = \sum_{i=1}^{m}\sum_{j=1}^{m} n_i n_j D_{ij} \tag{3}$$

3. Lattice diffusivity for SAC405

Although there is no direct experimental data for the diffusivity of SAC405, many researchers studied the diffusion behavior of tin, silver, copper and their interactions, as can be seen in Table 2.

By comparing the coefficients for different diffusion couples in Table 2 we can see that the interstitial diffusivity of copper in tin is far larger than that of the rest components (atomic radius of Cu is 1350 Å versus Sn 1450 Å). In other words, although the weight percentage of copper and silver are far less than tin, they still play a major role in the atomic diffusion and vacancy diffusion of SAC405.

Using Eq. (3), we can get an approximation for the lattice diffusivity of SAC405 based on the mole weight of each composition. The temperature dependent lattice diffusivity of SAC405 is finally expressed by

$$D^{l}_{\mathrm{SAC405}} = 5.20\times10^{-5}\ \mathrm{cm^2\ s^{-1}}\exp\left(-\frac{8.0\ \mathrm{Kcal\ mol^{-1}}}{RT}\right) \tag{4}$$

4. Grain boundary diffusivity

In polycrystalline metals the atoms are less regularly bonded along grain boundary. As a result, grain boundary energy is higher than regularly aligned lattice energy. As a result, these boundary atoms can easily break bonds with neighbors and can diffuse to another lattice site. Hence, the grain boundary diffusion controls the EM and TM process in solder alloys [7,8,28–36]. Exact mathematical solutions of grain boundary diffusion have been worked out by Whipple [37], and by Suzuoka [38], for two sets of boundary conditions. Whipple assumed that the surface concentration of the diffusant is maintained everywhere at some constant value (constant concentration source model), on the other hand Suzuoka's model is based upon the assumption that the thin uniform layer of material deposited on the surface of the solute diffuses into the sample, but without there being any diffusion at all within the layer parallel to the surface (instantaneous source model). Whipple's solutions [37] is given by

$$D_{gb}\delta = -\left(\frac{\partial \ln C}{\partial \ln x^{6/5}}\right)^{-5/3}\sqrt{\frac{4D_l}{t}}0.78^{5/3} \tag{5}$$

Suzuoka's solution [38,39] is given by

$$D_{gb}\delta = -\left(\frac{\partial \ln C}{\partial \ln x^{6/5}}\right)^{-5/3}\sqrt{\frac{4D_l}{t}}(0.72\beta^{0.008})^{5/3} \tag{6}$$

where D_{gb} is the grain boundary diffusivity, D_l is the lattice diffusivity, δ is the grain boundary width, t is the annealing time, C is the liquid tracer agent concentration in a section at a depth of x cm from the original surface, and β is given by

$$\beta = \frac{D_{gb}\delta}{2D_l\sqrt{D_l t}} \tag{7}$$

It has been reported that at room temperature, $D_{gb}/D_l \sim 10^9$ [6], the grain boundary width δ is about 5×10^{-8} cm [40]. By simple calculation we can find that Suzuoka's grain boundary solution is only a few percent different from Whipple's solution for SAC405

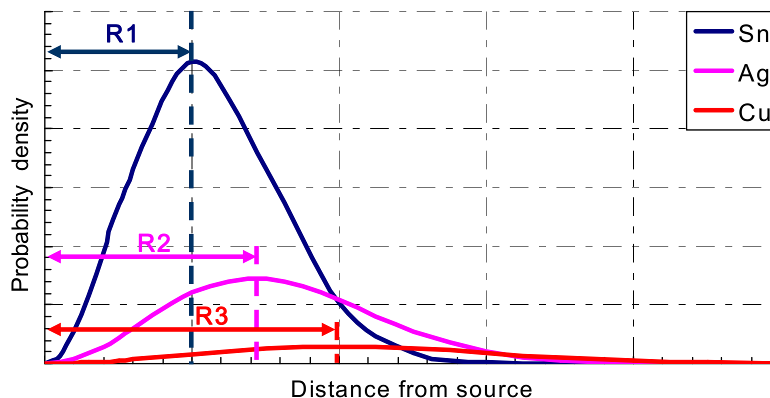

Fig. 2. Probability density for SAC405 spreading from an instantaneous point source.

Table 2
Relevant diffusion coefficient for tin–silver–copper diffusion system.

Solute	Solvent: Sn					
	wt%	mol%	D_0 (cm^2/s)	Q (Kcal mol^{-1})	Ref.	
Sn	95.50%	94.73%	$12.8^{+5.9}_{-4.1}$	26.0±0.4	Huang 1974[19]	Interstitial diffusivity
			N/A	25.6	Meakin 1960[11]	Sn (c axis)
			N/A	29.4		Sn (a axis)
Ag	4.00%	4.34%	7.10×10^{-3}	12.3±0.4	Dyson 1966[20]	Bulk diffusion of Ag in Sn
			N/A	16.8	Su 2002[21]	Ag_3Sn
Cu	0.50%	0.93%	2.4×10^{-3}	7.9	Dyson 1967[22]	Bulk diffusion of Cu in Sn
			2.6×10^{-5}	21.4	Flander 1997[23]	Cu_6Sn_5
			1.8×10^{-5}	12.9	Mei 1992[24]	IMC Cu-Sn
			N/A	20.1	Yoon 2003[25]	Spreading
			N/A	10.0		Immersing
			N/A	22.1	Pinizzotto 1993[26]	Cu_6Sn_5 at the Cu substrate interface
			N/A	12.2±3.8	Chason 1989[27]	Cu_6Sn_5 Sn Equilibrium
			N/A	20.8±1.0		Cu_6Sn_5 Sn Deficient

solder alloy. However, concerning its implicit form, Suzuoka's solution requires much more computational effort costs than Whipple's. Therefore, Whipple's solution is used in this work.

Both Levine and MacCallum [41] and Spindler and Nachtrieb [42] show that the relationship between $\ln C$ and $x^{6/5}$ is linear. This relationship was measured by Spindler and Nachtrieb [42] in the temperature range of 574–1046 °C. In the absence of more precise experimental data for SAC405, in this study, Spindler and Nachtrieb's data is assumed to hold for SAC405, which is given by,

$$\frac{d\ln C}{dx^{6/5}} = -88.67 \pm 18.36\ \mathrm{cm}^{-6/5} \tag{8}$$

The annealing time in Spindler and Nachtrieb [42] study was 10^6 s, which is comparable in magnitude to the typical electromigration and thermomigration testing on solder joints.

5. Monte Carlo simulations for Varying Microstructures

Solder alloys are polycrystalline materials with randomly oriented grains. According to Smith and Guttman [43] and Levine and MacCallum [41], the randomly oriented grains in a macroscopically homogeneous body are polyhedral and no one shape can be regarded as typical. The mean linear dimension, $\langle l \rangle$, of a grain can be established by a simple linear grain boundary intercept counting on a random two dimensional section of the body according to ASTM Standard E112. If λ is the total length of grain boundary trace exposed per unit area of a random section through the body, without any assumption regarding the actual shape of the grains or disposition of the boundaries, one can show that [41,43]

$$\lambda = \pi/2\langle l \rangle \tag{9}$$

A FORTRAN program has been coded to simulate diffusion in randomly oriented in SAC405 polycrystalline, taking into account lattice, and grain boundary diffusivity and microstructural topography. Random number sequences are generated to simulate the propagation of diffusion considering random grain orientation, grain size, grain shape, and activation energy of SAC405 polycrystalline. Fig. 3 shows some examples of microstructure models of different mesh density. Effective diffusivity is calculated for each

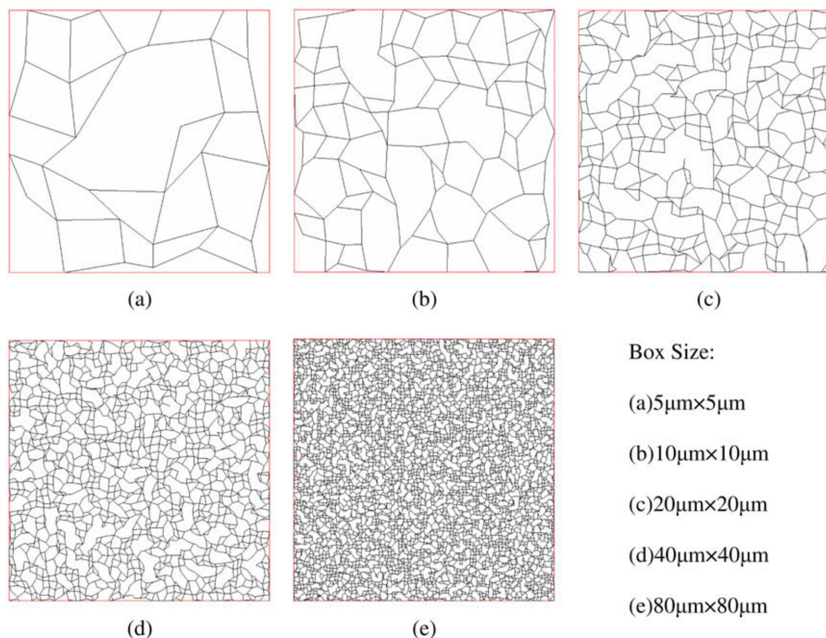

Fig. 3. Examples of microstructure models (average grain size: 1 μm).

randomly generated microstructure. By evaluating these stochastic values, temperature and grain size dependent diffusivity equations are determined.

In order to study mesh sensitivity of the proposed algorithm 5×5, 10×10, 20×20, 40×40 and 80×80 lattice meshes were used. 1000 simulations have been done for each mesh density, except for 80×80, to evaluate the total length of grain boundary per unit area. Fifty simulations were run for 80×80 lattice because of computational limitations. The results are plotted in Fig. 4, where λ is the total length of grain boundaries. For reference λ, once we know $\langle l \rangle$ for each microstructure, it can be obtained as is defined by Eq. (9). From Fig. 4 we can see that λ approaches to the reference ratio with the increasing mesh density. The difference between the calculated λ and the reference value of λ is due to the artificial boundary effect created by mesh sensitivity of the method. From Fig. 4 we can see that when we increase the mesh density to 40×40, the artificial grain boundary induced error is negligible. In other words, a mesh of 40×40 can effectively simulate the distribution of polycrystalline microstructure. Fig. 5 shows estimated diffusivity as a function of replication number. From this figure we can see that when the replication number is larger than 500 times, both the estimated diffusivity and variance remain the same, which indicate that the Monte Carlo algorithm used in this work is converging and stable.

5. Discussion of results

Computing time rises dramatically with the increasing lattice density. For example, with a 3.2 GHz Xeon CPU, it takes just a few minutes to finish a 1000-loop for a model with mesh density of 20×20. As we increase the mesh density to 40×40, it takes about 40 hours to finish a 1000-loop simulation. When it comes to 80×80, the computing time needed is more than 6700 h. However, as we have shown in Fig. 4, it will not yield a significant improvement in accuracy by increasing the mesh density from 40×40 to 80×80. Therefore, 40×40 lattice boxes are adopted in our simulation for effective diffusivity simulations.

The last five digits of Real Time Clock (RTC) value are used to generate random number seed for every loop. RTC is a computer clock that keeps track of the current time. The method of using CPU time to generate random seeds comes from error theory. According to error theory [44], the values composed by the last few digits of CPU time in a big enough time span is random. In this way we can randomize the initial status of our repetitive simulations. We record the random number seed for every loop so that we can repeat any single loop if needed although the seed itself is unpredictable before simulation.

In this work, effective diffusivity is calculated for seven levels of temperatures: $T = 26.85\,°C$ (300 K), 46.85 °C (320 K), 66.85 °C (340 K), 86.85 °C (360 K), 106.85 °C (380 K), 126.85 °C (400 K),

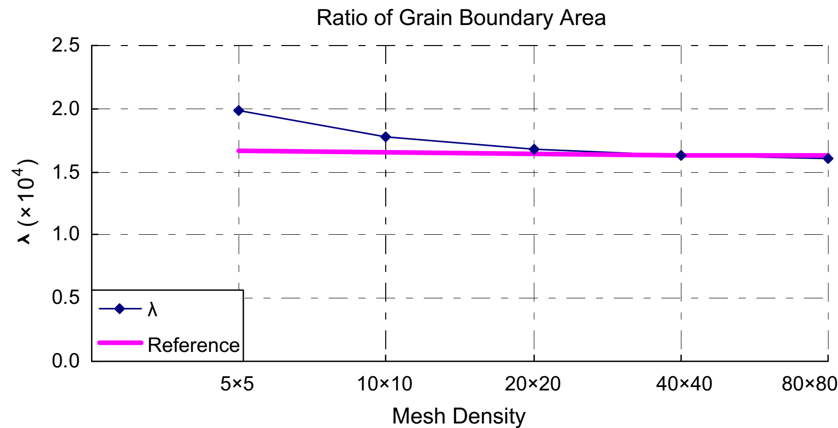

Fig. 4. Ratio of grain boundary area.

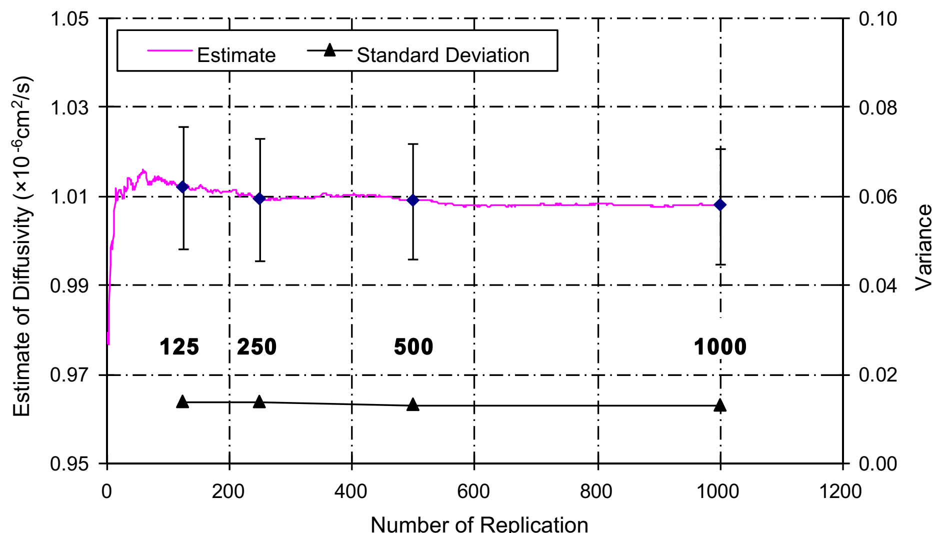

Fig. 5. Stability of the Monte Carlo simulation result (mesh density: 40×40; temperature: 26.85 °C (300 K); average grain size: 1 μm).

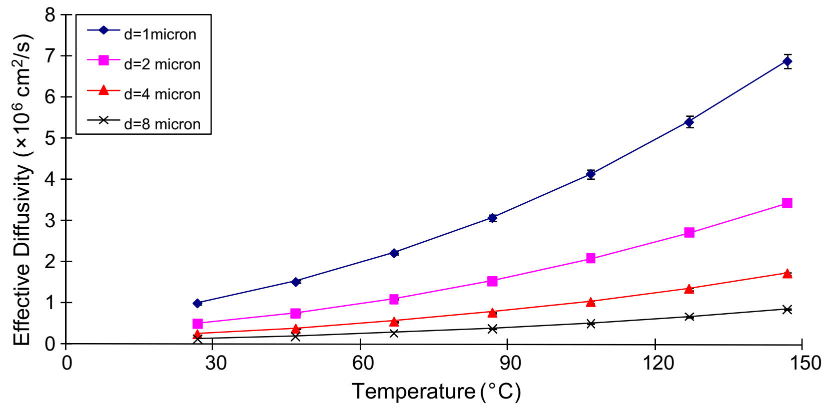

Fig. 6. The relationship of effective diffusivity versus temperature and average grain size.

and 146.85 °C (420 K). For each temperature level, 4 different grain sizes are used in the study: $d = 1$ μm, 2 μm, 4 μm and 8 μm. Using six different temperatures and 4 different grain sizes the grid shown in Fig. 6 was obtained. The effective diffusivity values needed for the FEM simulations can be obtained from this Fig. 6. The details of the data plotted in Fig. 6 are given in Appendix. Based on these data, an empirical equation which describes the relationship of effective diffusivity and grain boundary diffusivity, can be obtained as Eq. (10),

$$D_{effective} = 0.69\frac{\delta}{d}D_{gb} \quad (10)$$

Eq. (10) has a form similar to Hart's relationship[45], which has the following form

$$D_{effective} = D_l + \frac{\delta}{d}D_{gb} \quad (11)$$

As we mentioned before, for solder alloys, the contribution of lattice diffusion, D_l, to effective diffusion is negligible, since lattice diffusivity is nine orders of magnitude smaller than grain boundary diffusivity. Therefore, Hart's model basically uses the product of grain boundary diffusivity and the fraction of grain boundary area over the whole cross section area as the effective diffusivity. It doesn't consider the randomness of the microstructure. Hart's model provides a fair approximation only when the grain is evenly distributed. According to our study, Hart model over-estimates the diffusion by 45%, which results in a reduction factor of 0.69 as seen in Eq. (10).

Ye [7] and Lin [8], assumed atomic diffusivity of SAC405 to be 2.97×10^{-11} cm^2/s at 300 K, $d = 0.3$ μm grain size based on premise that pure tin grain boundary diffusivity will govern the diffusion in SAC405. However, from Fig. 6 we can see that the calculated effective diffusivity is in the magnitude of 10^{-7}–10^{-6} cm^2/s. At 300 K, $d = 1$ μm, the effective diffusivity is calculated to be 2.23×10^{-6} cm^2/s, which is five orders larger than the value adopted by Ye [7] and Lin [8]. Considering the diffusivity of Ag in Sn and Cu in Sn are both more than six orders of magnitude larger than the self diffusivity of pure tin. In SAC405 copper and silver are the major diffusants; therefore these impurities govern the effective diffusivity of the alloy.

6. Conclusions

In this paper a stochastic method is proposed to find the effective diffusivity of lead free solder alloy, SAC405, using the experimental data available in the literature and Monte Carlo simulations. Based on a considerably large sample space, the effective diffusivity is obtained at seven levels of temperature and four different grain sizes. This map covers most of the diffusivity values that may be need for most FEM analysis of nanoelectronics solder joints subjected to thermomigration and electromigration.

Our work shows that the assumption of tin grain boundary diffusivity dominates SAC effective diffusivity significantly underestimates the value of SAC diffusivity.

It is also shown that Hart's model is conservative in revealing the relationship between effective diffusivity and grain boundary diffusivity. By using Hart's model, the effective diffusivity is about 45% overestimated. A reduction factor of 0.69 is suggested to modify Hart's effective diffusivity model.

Appendix

See Tables A1–A7.

Table A1
Diffusion coefficient for different grain size at 300 K.

Grain size (micron)		λ	λ_{Ref}	D_l (cm^2/s)	D_{gb} (cm^2/s)	$D_{effective}$ (cm^2/s)
$d = 1$	Average	1.63×10^4	1.64×10^4	3.11×10^{-10}	6.51×10^{-3}	2.23×10^{-6}
	StdDev	1.24×10^2	5.03×10^1	3.14×10^{-12}	3.82×10^{-5}	5.13×10^{-8}
$d = 2$	Average	8.16×10^3	8.18×10^3	3.12×10^{-10}	6.51×10^{-3}	1.11×10^{-6}
	StdDev	7.53×10	3.04×10^1	3.02×10^{-12}	3.82×10^{-5}	2.89×10^{-8}
$d = 4$	Average	4.08×10^3	4.09×10^3	3.11×10^{-10}	6.52×10^{-3}	5.56×10^{-7}
	StdDev	2.83×10^1	1.34×10^1	3.38×10^{-12}	3.88×10^{-5}	1.34×10^{-8}
$d = 8$	Average	2.04×10^3	2.05×10^3	3.11×10^{-10}	6.51×10^{-3}	2.76×10^{-7}
	StdDev	1.65×10^1	6.79×10^0	2.99×10^{-12}	3.21×10^{-5}	7.41×10^{-9}

Table A2
Diffusion coefficient for different grain size at 320 K.

Grain size (micron)		λ	λ_{Ref}	D_l (cm^2/s)	D_{gb} (cm^2/s)	$D_{effective}$ (cm^2/s)
d = 1	Average	1.63×10^4	1.64×10^4	1.45×10^{-10}	4.47×10^{-3}	1.53×10^{-6}
	StdDev	1.29×10^2	5.41×10^1	1.43×10^{-12}	2.54×10^{-5}	3.75×10^{-8}
d = 2	Average	8.16×10^3	8.18×10^3	1.45×10^{-10}	4.47×10^{-3}	7.63×10^{-7}
	StdDev	6.73×10^1	2.75×10^1	1.42×10^{-12}	2.31×10^{-5}	1.52×10^{-8}
d = 4	Average	4.08×10^3	4.09×10^3	1.45×10^{-10}	4.47×10^{-3}	3.84×10^{-7}
	StdDev	3.53×10^1	1.39×10^1	1.39×10^{-12}	2.43×10^{-5}	9.64×10^{-9}
d = 8	Average	2.04×10^3	2.05×10^3	1.45×10^{-10}	4.47×10^{-3}	1.90×10^{-7}
	StdDev	1.88×10^1	6.95×10^0	1.38×10^{-12}	2.30×10^{-5}	5.70×10^{-9}

Table A3
Diffusion coefficient for different grain size at 340 K.

Grain size (micron)		λ	λ_{Ref}	D_l (cm^2/s)	D_{gb} (cm^2/s)	$D_{effective}$ (cm^2/s)
d = 1	Average	1.63×10^4	1.64×10^4	3.11×10^{-10}	6.51×10^{-3}	2.23×10^{-6}
	StdDev	1.24×10^4	5.03×10^1	3.14×10^{-12}	3.82×10^{-5}	5.13×10^{-8}
d = 2	Average	8.16×10^3	8.18×10^3	3.12×10^{-10}	6.51×10^{-3}	1.11×10^{-6}
	StdDev	7.53×10^1	3.04×10^1	3.02×10^{-12}	3.82×10^{-5}	2.89×10^{-8}
d = 4	Average	4.08×10^3	4.09×10^3	3.11×10^{-10}	6.52×10^{-3}	5.56×10^{-7}
	StdDev	2.83×10^1	1.34×10^1	3.38×10^{-12}	3.88×10^{-5}	1.34×10^{-8}
d = 8	Average	2.04×10^3	2.05×10^3	3.11×10^{-10}	6.51×10^{-3}	2.76×10^{-7}
	StdDev	1.65×10^1	6.79×10^0	2.99×10^{-12}	3.21×10^{-5}	7.41×10^{-9}

Table A4
Diffusion coefficient for different grain size at 360 K.

Grain size (micron)		λ	λ_{Ref}	D_l (cm^2/s)	D_{gb} (cm^2/s)	$D_{effective}$ (cm^2/s)
d = 1	Average	1.63×10^4	1.64×10^4	6.12×10^{-10}	9.09×10^{-3}	3.08×10^{-6}
	StdDev	1.19×10^2	4.90×10^1	5.34×10^{-12}	4.42×10^{-5}	8.13×10^{-8}
d = 2	Average	8.18×10^3	8.17×10^3	6.13×10^{-10}	9.08×10^{-3}	1.54×10^{-6}
	StdDev	6.33×10^1	2.65×10^1	5.36×10^{-12}	5.03×10^{-5}	3.53×10^{-8}
d = 4	Average	4.09×10^3	4.09×10^3	6.12×10^{-10}	9.09×10^{-3}	7.73×10^{-7}
	StdDev	3.37×10^1	1.41×10^1	5.69×10^{-12}	5.08×10^{-5}	2.01×10^{-8}
d = 8	Average	2.04×10^3	2.04×10^3	6.13×10^{-10}	9.09×10^{-3}	3.87×10^{-7}
	StdDev	1.70×10^1	7.04×10^0	5.13×10^{-12}	4.84×10^{-5}	9.64×10^{-9}

Table A5
Diffusion coefficient for different grain size at 380 K.

Grain size (micron)		λ	λ_{Ref}	D_l (cm^2/s)	D_{gb} (cm^2/s)	$D_{effective}$ (cm^2/s)
d = 1	Average	1.63×10^4	1.64×10^4	1.13×10^{-9}	1.23×10^{-2}	$4.15 \times 10^{--6}$
	StdDev	1.49×10^2	6.42×10^1	8.90×10^{-12}	6.06×10^{-5}	1.05×10^{-7}
d = 2	Average	8.18×10^3	8.18×10^3	1.12×10^{-9}	1.23×10^{-2}	2.09×10^{-6}
	StdDev	6.35×10^1	2.60×10^1	8.36×10^{-12}	6.46×10^{-5}	5.28×10^{-8}
d = 4	Average	4.09×10^3	4.09×10^3	1.12×10^{-9}	1.22×10^{-2}	1.03×10^{-6}
	StdDev	3.77×10^1	1.52×10^1	1.03×10^{-12}	6.58×10^{-5}	2.80×10^{-8}
d = 8	Average	2.04×10^3	2.04×10^3	1.12×10^{-9}	1.22×10^{-2}	5.18×10^{-7}
	StdDev	1.58×10^1	6.30×10^0	9.27×10^{-12}	6.56×10^{-5}	1.19×10^{-8}

Table A6
Diffusion coefficient for different grain size at 400 K.

Grain size (micron)		λ	λ_{Ref}	D_l (cm^2/s)	D_{gb} (cm^2/s)	$D_{effective}$ (cm^2/s)
d = 1	Average	1.63×10^4	1.63×10^4	1.93×10^{-9}	1.60×10^{-2}	5.41×10^{-6}
	StdDev	1.36×10^2	6.12×10^1	1.61×10^{-11}	8.16×10^{-5}	1.44×10^{-7}
d = 2	Average	8.18×10^3	8.17×10^3	1.93×10^{-9}	1.60×10^{-2}	2.71×10^{-6}
	StdDev	7.01×10^1	3.02×10^1	1.71×10^{-11}	8.77×10^{-5}	6.18×10^{-8}
d = 4	Average	4.09×10^3	4.09×10^3	1.93×10^{-9}	1.60×10^{-2}	1.35×10^{-6}
	StdDev	3.47×10^1	1.37×10^1	1.63×10^{-11}	8.91×10^{-5}	3.60×10^{-8}
d = 8	Average	2.04×10^3	2.04×10^3	1.93×10^{-9}	1.60×10^{-2}	6.77×10^{-7}
	StdDev	1.58×10^1	6.46×10^0	1.36×10^{-11}	7.88×10^{-5}	1.67×10^{-8}

Table A7
Diffusion coefficients for different grain size at 420 K.

Grain size (micron)		λ	λ_{Ref}	D_l (cm^2/s)	D_{gb} (cm^2/s)	$D_{effective}$ (cm^2/s)
d = 1	Average	1.63×10^4	1.64×10^4	3.16×10^{-9}	2.04×10^{-2}	6.89×10^{-6}
	StdDev	1.54×10^2	6.00×10^1	2.07×10^{-11}	1.01×10^{-4}	1.80×10^{-7}
d = 2	Average	8.17×10^3	8.17×10^3	3.16×10^{-9}	2.04×10^{-2}	3.43×10^{-6}
	StdDev	6.13×10^1	2.69×10^1	2.12×10^{-11}	9.20×10^{-5}	8.08×10^{-8}
d = 4	Average	4.09×10^3	4.09×10^3	3.15×10^{-9}	2.04×10^{-2}	1.73×10^{-6}
	StdDev	3.12×10^1	1.31×10^1	2.37×10^{-11}	1.02×10^{-4}	3.70×10^{-8}
d = 8	Average	2.04×10^3	2.04×10^3	3.15×10^{-9}	2.04×10^{-2}	8.60×10^{-7}
	StdDev	1.49×10^1	5.65×10^0	2.55×10^{-11}	1.16×10^{-4}	2.02×10^{-8}

References

[1] W.J. Callister, Materials Science and Engineering: An Introduction, fouth ed., John Wiley and Sons, 1996.
[2] R.J. Gleixner, W.D. Nix, An Analysis of Void Nucleation in Passivated Interconnect Lines Due to Vacancy Condensation and Interface Contamination, in: Thin Films: Materials Reliability in Microelectronics VI, San Fransisco, CA, 1996, pp. 475–480.
[3] R.J. Gleixner, B.M. Clemens, W.D. Nix, Journal of Materials Research 12 (8) (1997) 10.
[4] C. Basaran, S. Li, M.F. Abdulhamid, Journal of Applied Physics 103 (12) (2008) 123520–123529.
[5] C. Basaran, S. Nie, International Journal of Damage Mechanics 13 (3) (2004) 205–223.
[6] P. Singh, M. Ohring, Journal of Applied Physics 56 (4) (1984) 899–907.
[7] H. Ye, Mechanical Behavior of Microelectronics and Power Electronics Solder Joints under High Current Density: Analytical Modeling and Experimental Investigation, in: Department of Civil, Structural, and Environmental Engineering, University at Buffalo, State University of New York: Buffalo, 2004, p. 297.
[8] M. Lin, A damage mechanics framework for electromigration failure, in: Department of Civil, Structural and Environmental Engineering, University at Buffalo, State University of New York: Buffalo, New York, 2006, p. 262.
[9] M. Abdulhamid, C. Basaran, ASME Journal of Electronic Packaging 131 (12) (2009) 011002.
[10] S. Li, M.F. Abdulhamid, C. Basaran, Mean time to failure estimation for low temperature electromigration and thermomigration, 2007.
[11] S.L. Allen et al., Journal of Materials Research 19 (5) (2004) 8.
[12] N. Dariavach et al., Journal of Electronic Materials 35 (7) (2006) 1581–1592.
[13] S. Gee et al., Mean Time To Failure in Wafer Level-CSP Packages with SnPb and SnAgCu Solder Bumps, in: International Wafer-Level Packaging Conference, San Jose, CA, USA, 2005.
[14] L. Xu et al., Journal of Electronic Materials 35 (12) (2006) 2116–2125.
[15] W. Metropolis, S. Ulam, Journal of the American Statistical Association 44 (247) (1949) 335–341.
[16] G.S. Fisherman, Monte Carlo: Concepts, Algorithms, and Applications, Springer-Verlag, New York, 1995.
[17] A. Einstein, Annalen der Physik 17 (1905) 12.
[18] M.E. Glicksman, Diffusion in Solids: Field Theory, Solid-State Principles, and Applications, John Wiley and Sons, Inc., 2000. p. 472.
[19] F.H. Huang, H.B. Huntington, Physical Review B 9 (4) (1974) 1479.
[20] B.F. Dyson, Journal of Applied Physics 37 (6) (1966) 2375–2377.
[21] T.L. Su et al., Journal of Materials Engineering and Performance 11 (2002) 365–368.
[22] B.F. Dyson, T.R. Anthony, D. Turnbull, Journal of Applied Physics 38 (8) (1967) 3408.
[23] D. Flanders, E. Jacobs, R. Pinizzotto, Journal of Electronic Materials 26 (7) (1997) 883–887.
[24] Z. Mei, A. Sunwoo, J. Morris, Metallurgical and Materials Transactions A 23 (3) (1992) 857–864.
[25] J.-W. Yoon, C.-B. Lee, S.-B. Jung, Journal of Electronic Materials 32 (11) (2003) 1195–1202.
[26] R.F. Pinizzotto et al. The dependence of the activation energies of intermetallic formation on the composition of composite Sn/Pb solders, in: Reliability Physics Symposium, 1993. 31st Annual Proceedings, International, 1993.
[27] M. Chason, J. Hong. Kinetic interactions of copper, lead and tin on solder coated PC boards studied using X-ray diffraction, in: Electronic Manufacturing Technology Symposium, 1989, Proceedings Seventh IEEE/CHMT International, 1989.
[28] H. Ye, C. Basaran, D.C. Hopkins, International Journal of Solids and Structures 40 (15) (2003) 4021–4032.
[29] H. Ye, C. Basaran, D.C. Hopkins, Numerical simulation of stress evolution during electromigration in IC interconnect lines. Components and Packaging Technologies, IEEE Transactions on [see also Components, Packaging and Manufacturing Technology, Part A: Packaging Technologies, IEEE Transactions on] 26(3) (2003) 673–681.
[30] C. Basaran, M. Lin, H. Ye, International Journal of Solids and Structures 40 (26) (2003) 7315–7327.
[31] H. Ye, C. Basaran, D.C. Hopkins, International Journal of Solids and Structures 40 (26) (2003) 7269–7284.
[32] H. Ye, D.C. Hopkins, C. Basaran, Microelectronics Reliability 43 (12) (2003) 2021–2029.
[33] H. Ye, C. Basaran, D.C. Hopkins, International Journal of Solids and Structures 41 (9-10) (2004) 2743–2755.
[34] M. Lin, C. Basaran, Computational Materials Science 34 (1) (2005) 82–98.
[35] H. Ye, C. Basaran, D.C. Hopkins, International Journal of Damage Mechanics 15 (1) (2006) 41–67.
[36] C. Basaran, M. Lin, International Journal of Materials and Structural Integrity 1 (2007) 16–39.
[37] R.T.P. Whipple, Philosophical Magazine 45 (1954) 12.
[38] T. Suzuoka, Journal of the Physical Society of Japan 19 (6) (1964) 13.
[39] A.D.L. Claire, British Journal of Applied Physics website 14 (6) (1963) 6.
[40] J.C. Fisher, Journal of Applied Physics 22 (1) (1951) 74–77.
[41] H.S. Levine, C.J. MacCallum, Journal of Applied Physics 31 (3) (1960) 5.
[42] P. Spindler, K. Nachtrieb, Metallurgical and Materials Transactions A 9 (6) (1978) 763–767.
[43] C.S. Smith, L. Guttman, Transactions of ASME 197 (1953) 12.
[44] T.H. Wonnacott, R.J. Wonnacott, Introductory Statistics, fifth ed., Wiley, 1990. p. 736.
[45] E.W. Hart, Acta Metallurgica 5 (10) (1957) 597.